SUPPLEMENTAL INFORMATION

Descending control of neural bias and selectivity in a spatial attention network: rules and mechanisms

Shreesh P. Mysore*†, Eric I. Knudsen

SUPPLEMENTAL DATA

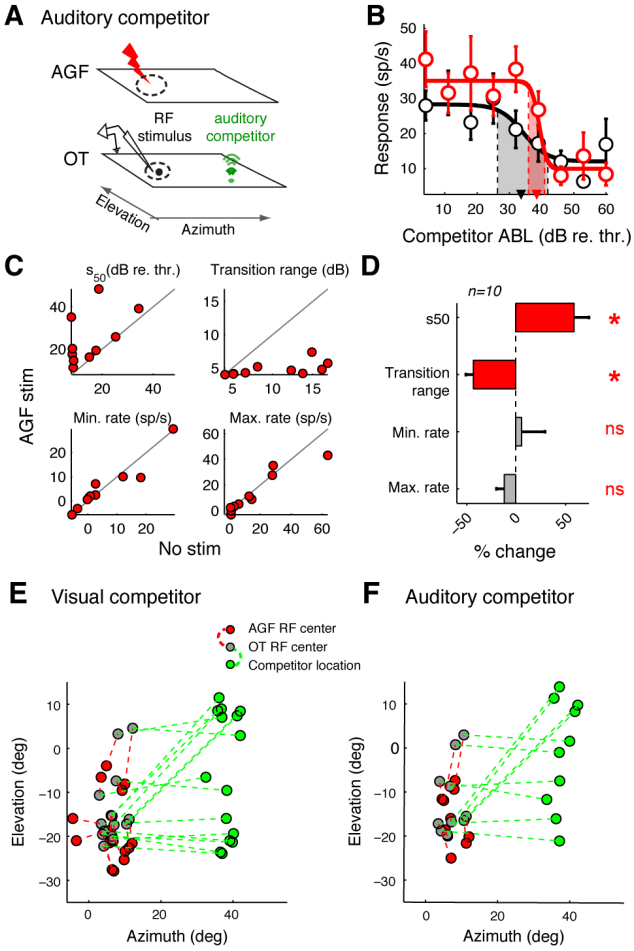

Figure S1 (related to Fig. 1). Effects of spatially congruent AGF microstimulation on multimodal competition in the OTid, and maps of AGF receptive fields, OT receptive fields, and competitor locations from experiments in Figure 1.

(A-D) Experiments with an auditory competitor; same conventions as in Figure 1. (A) Schematic of experimental protocol. (B) Responses of an OTid neuron to the competition protocol without (black) and with spatially congruent AGF microstimulation (red). Distance between centers of OTid and AGF RFs = 5°; loom speed (strength) of RF stimulus = 4.8°/s; strength of microstimulation current = 20 mA. (C) Scatter plots of values of sigmoidal parameters without vs. with aligned AGF microstimulation. (D) Population summary (n=10 neurons from 3 birds). S_{50}: t-test, p=0.022, t_9 = 2.63; transition range: t-test, $p<10^{-3}$, t_9= -5.69; minimum rate: rank-test, p=1, signed rank = 27; maximum rate: rank-test, p= 0.27, signed rank=15.

(E-F) Locations of the receptive field centers of OTid neurons, the corresponding microstimulation sites in the AGF, and the locations of the competitors. (E) Data from experiments in Figures 1A-D (visual competitor). Average distance between the centers of OTid and AGF RFs = 5° ± 0.8° (mean ± s.e.m); average distance between OTid RF center and competitor location = 35° ± 1.2°. Average loom speed (strength) of the RF stimulus = 6.9 °/s ± 0.5 °/s (mean ± s.e.m). Average strength of microstimulation current = 13.5 ± 1.3 mA. (F)

Data from experiments in panels A-D (auditory competitor). Average distance between centers of OTid and AGF RFs = 4.7° ± 1.2° (mean ± s.e.m); average distance between OTid RF center and competitor location = 34.5° ± 1.6°. Average loom speed (strength) of the RF stimulus = 6.1 °/s ± 0.8°/s. Average strength of microstimulation current = 12.2 ± 1.6 mA.

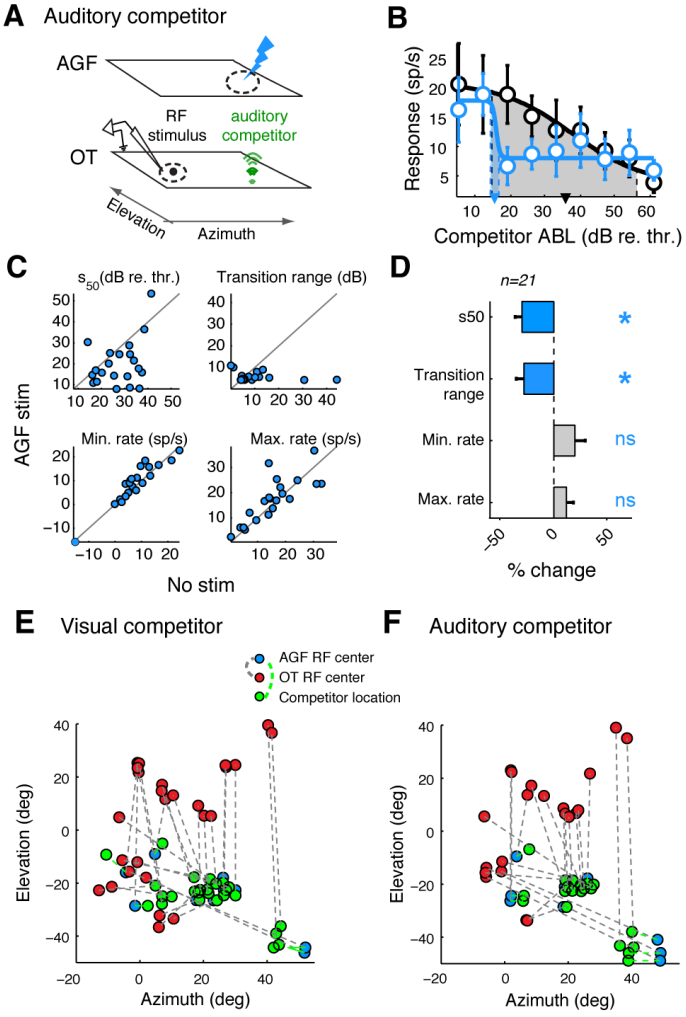

Figure S2 (related to Fig. 2). Effects of spatially non-congruent AGF microstimulation on multimodal competition in the OTid, and maps of AGF receptive fields, OT receptive fields, and competitor locations from experiments in Figure 2.

(A-D) Auditory competitor; same conventions as in Figure 2. (A) Schematic of experimental protocol. (B) Responses of an OTid neuron to the competition protocol without (black) and with spatially congruent AGF microstimulation (blue). Distance between OTid RF center and AGF RF center/location of competitor = 48°; loom speed (strength) of RF stimulus = 10°/s; strength of microstimulation current = 16 mA. (C) Scatter plots of values of sigmoidal parameters without vs. with non-aligned AGF microstimulation. (D) Population summary (n=21 neurons from 6 birds). S_{50}: t-test, p=0.002, t_{20}=-3.65; transition range: rank-test, p=0.005, signed rank = 29; minimum rate: rank-test, p=0.23, signed rank = 82; maximum rate: rank-test, p= 0.11, signed rank = 64.

(E-F) Same conventions as in Figure S1. (E) Data from experiments in Figures 2A-D (visual competitor). Average distance between OTid RF center and AGF RF center/location of competitor = 37.3° ± 3.3°. Average loom speed (strength) of the RF stimulus = 7.7 °/s ± 0.35 °/s. Average strength of microstimulation current = 16.5 ± 0.7 mA. (F) Data from experiments in panels A-D (auditory competitor). Average distance between OTid RF center and AGF RF center/location of competitor = 40° ± 4°. Average loom speed (strength) of the RF stimulus = 7.8 °/s ± 0.4°/s. Average strength of microstimulation current = 15.6 ± 0.7 mA.

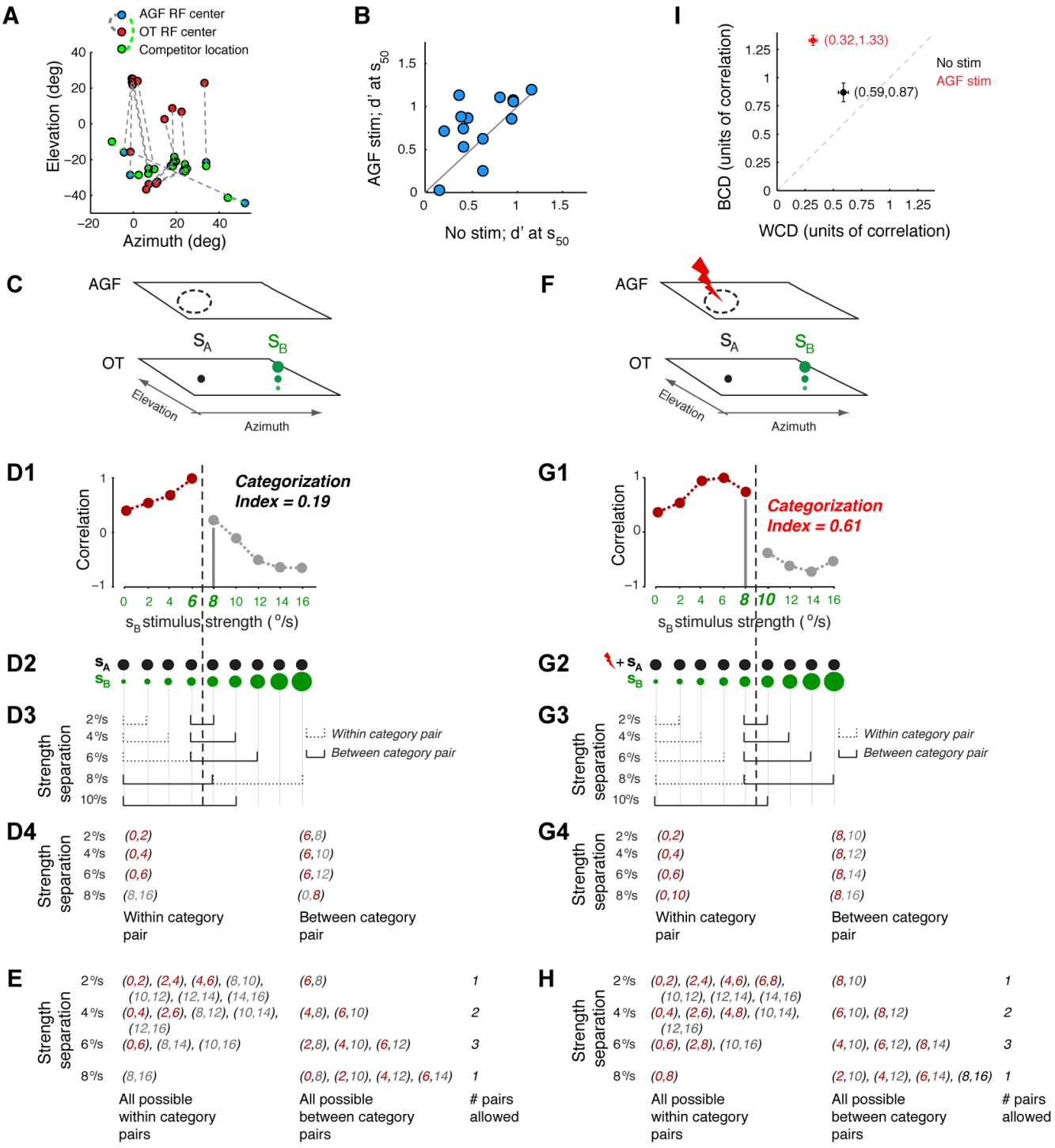

Figure S3 (related to Figs. 3 and 7). Effect of AGF microstimulation on neurons encoding the competitor stimulus, and calculation of the categorization index.

(A) Locations of the receptive field centers of OTid neurons, the microstimulation sites in the AGF, and the locations of the competitors. from the experiments in Figure 3A-D. Conventions same as in Figure S2. **(B)** For experiments in Figure 3A-D: Effect of AGF microstimulation on the discriminability (d') of the highest priority stimulus when competing stimuli have very similar priorities, i.e., with the stimuli just straddling the category boundary. Same conventions as in Figure 7.

(C-E) Calculation of the categorization index for the response profile at the bottom panel of Figure 3F (no stimulation condition). **(C)** Schematic of stimulus protocol (modified from Fig. 3E) showing the stimulus of fixed strength (in black; referred to as s_A for clarity), and the stimulus of systematically varying strength (in

green; referred to as s_B). **(D)** *D1.* Response profile reproduced from Figure 3F, bottom panel. Dashed vertical line represents the category boundary, the strength of s_B that causes the change in response correlation. In brown: category 1 (s_A is the highest priority stimulus). In gray: category 2 (s_B is the highest priority stimulus). *D2.* Schematic of the strengths of s_A and s_B tested in the stimulus protocol. *D3.* Examples of within-category and between-category stimulus pairs corresponding to different values of separation in the strength of s_B. For the separation of 10 °/s, a within category stimulus pair does not exist. *D4.* The stimulus pairs from D3 represented as Cartesian pairs; the two values within each pair represent the strengths of s_B. Text in brown corresponds to s_B values in category 1; text in gray corresponds to s_B values in category 2. **(E)** Table showing all possible within-category and between-category stimulus pairs for different strength separations. The rightmost column lists the number of allowed stimulus pairs corresponding to each strength separation.
(F-H) Calculation of the categorization index for the response profile at the bottom panel of Figure 3H (AGF stimulation condition). Same conventions as in C-E.
(**I**) WCD and BCD values (mean ± s.e.m) obtained using a Monte Carlo simulation (N=1000; Experimental Procedures). Pairs represent the mean (WCD, BCD) values calculated for the response profiles in the bottom panels in Figure 3F (black; no stimulation) and 3H (red; AGF stimulation). Dashed line represents points for which WCD = BCD (categorization index =0).

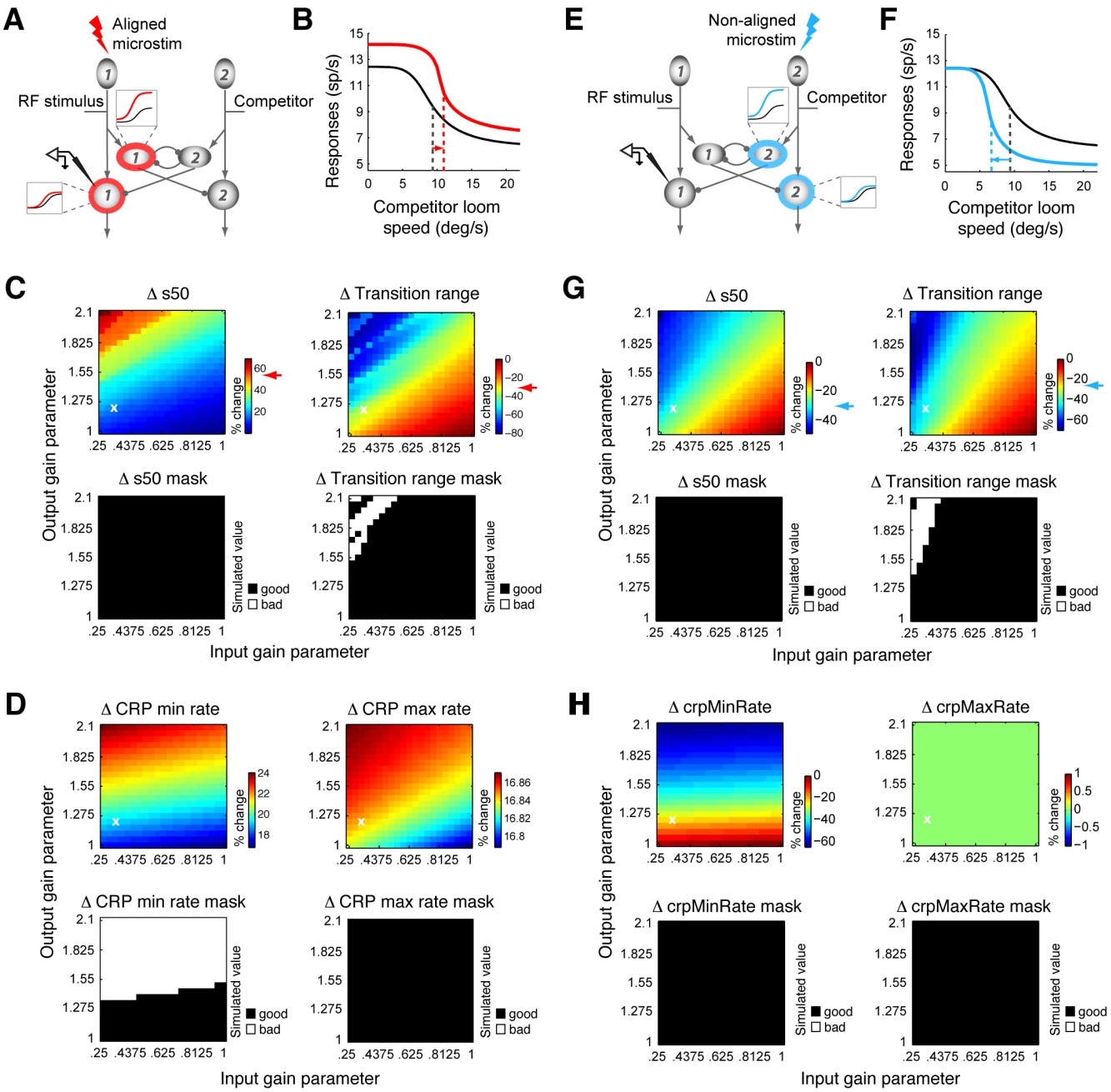

Figure S4 (related to Fig. 6). Computational model III ("mixed" model): Gain modulation of units inside, as well as of those outside, the inhibitory feedback loop robustly reproduces the experimental effects of AGF microstimulation.

The AGF modulates the gain of Imc and OTid units in a space-specific manner. Same conventions as in Figure 6. For all panels, AGF→OTid input gain parameter = 0.7, response gain parameter = 1.03 (values chosen to match experimentally observed results; Winkowski and Knudsen, 2008)

(**A-D**). Effects of aligned AGF stimulation (red icons and data). **(A)** Insets: Visual mnemonic illustrating multiplicative gain modulation of Imc and OT responses by AGF microstimulation. Shown are schematic responses of an Imc (or OTid) unit to a single stimulus inside the RF, without (black) and with (red) microstimulation. X-axis, strength of RF stimulus; y-axis, firing rate. **(B)** AGF→Imc input gain parameter = 0.325, response gain parameter = 1.22 (same values of AGF→OTid gain parameters as in Figure 5b, and correspond to the white 'x' in C; top panels). **(C-D)** A wide range of values of the input and response

multiplicative gain factors yielded results that were consistent with experimental results. Same conventions as in Figure 6C-D.

(**E-H**) Effects of non-aligned stimulation (AGF RF non-aligned with OTid RF, but aligned with location of the competitor; blue icons and data). Same conventions as in Figure 6E-H. (F) AGF→Imc input gain parameter = 0.325, response gain parameter = 1.22.

Model III: (Supplemental text related to Fig. S4.) In the interest of completeness, we tested whether a "mixed" model in which AGF microstimulation modulated loom speed responses in *both* the OTid and the Imc could also account for the experimentally observed effects on CRPs in the OTid (Fig. S4). We found that the mixed model also successfully reproduced the key results of aligned as well as non-aligned AGF microstimulation. The nature of the modulation by the AGF was multiplicative at both sites and was space-specific, as in models I and II. For these simulations, the values of the input and response multiplicative gain parameters at the OTid were fixed at 0.7 and 1.03, respectively. These values were chosen because they produced effects on single-stimulus, strength-response functions in the OTid that matched the average experimentally observed effects of aligned AGF microstimulation (Winkowski and Knudsen, 2008). The input and response multiplicative gain parameters at the Imc were varied over a range of values as in model II (Fig. 6).

When we simulated the effects of aligned AGF microstimulation on OTid CRPs, we found that the mixed model successfully reproduced the key results (Fig. S4A-D). Rightward shifts of CRPs and a narrowing of transition ranges were observed over a large range of values of the Imc gain parameters (Fig. S4C). The primary consequence of including AGF modulation of the OTid in this model was an increase in CRP min and max rates. These increases were well within the experimentally observed ranges (Fig. S4D).

When we simulated the effects of non-aligned AGF microstimulation on OTid CRPs, we found that the effects (Fig. S4E-H) were identical to those found with model II (Fig. 6E-H). The reason for this becomes clear upon closer examination of the circuit model (Fig. S4E). Because the recording site in the OTid (site #1) is distant from the OTid site of direct AGF-dependent modulation (site #2), the recording site is affected only by the AGF's modulation of the Imc (site #2; as described in model II), but not by the AGF's direct modulation of OTid site #1. Thus, the mixed model also accounted for the effects of non-aligned AGF microstimulation.

SUPPLEMENTAL EXPERIMENTAL PROCEDURES

Animals. Experiments were performed on 8 head-fixed, non-anesthetized, adult barn owls (*Tyto alba)*. Both male and female birds were used. All procedures for bird care and use were approved by the Stanford University Institutional Animal Care and Use Committee and were in accordance with the National Institutes of Health and the Society for Neuroscience guidelines for the care and use of laboratory animals. Owls were group housed in enclosures within the vivarium, each containing 3-5 birds. The light/dark cycle was 12 hrs/12 hrs.

Neurophysiology. Experiments were performed following protocols that have been described previously (Mysore et al., 2010, 2011; Mysore and Knudsen, 2013). Briefly, epoxy-coated tungsten microelectrodes (A-M Systems, 250μm diameter, 1-5 MΩ at 1 kHz) were used to record single and multi-units extracellularly. A mixture of isofluorane (1.5-2%) and nitrous oxide/oxygen (45:55 by volume) was used at the start of the experiment to anesthetize the bird while it was secured in the experimental rig (a 20 minute period of initial set-up). Isofluorane was turned off immediately after the bird was secured and was never turned back on for the remainder of the experiment. Frequently, nitrous oxide was also turned off at this point, but in several experiments, it was left on for a few hours if the bird's temperament necessitated it (some birds were calm when restrained, while others were not). However, it was turned off at least 30 minutes before the recording session. Our recordings were performed between 8-12 hours after initial set-up (the time required for positioning the electrodes). Since recovery from isofluorane occurs well under 30 minutes after it is turned off, and recovery from nitrous oxide occurs within a minute (the bird stands up and flies away if freed from restraints), recordings were made in animals that were not anesthetized.

AGF microstimulation. Electrical microstimulation of the AGF followed the protocol described previously (Mysore and Knudsen, 2013; Winkowski and Knudsen, 2006). Briefly, an epoxy-coated tungsten microelectrode (FHC; 1 MΩ at 1kHz) was used to identify a "patch" of tissue in the AGF with consistent spatial tuning. This was defined as a 300 μm span along the dorsoventral penetration path of the electrode, such that the locations of neuronal visual receptive fields measured at the top, middle and bottom of the span were not significantly different (centered within ± 5 °). Electrical stimulation consisted of biphasic 200 Hz pulses, delivered for 25 ms (Grass S88 stimulator with two Grass stimulus isolation units PSIU-6). AGF stimulation was delivered starting at 0 ms (i.e., simultaneously with stimulus onset) in all cases except when an auditory stimulus was congruent with it; in that case, it was delivered at -25 ms (25 ms before onset of the auditory stimulus) (Mysore and Knudsen, 2013; Winkowski and Knudsen, 2006). Current levels used (5-25 μA) were far below those required to elicit small amplitude eye deflections (100-600 μA); current amplitudes were measured from the voltage drop across a 1 kΩ resistor in the return path of the current source.

Site selection for recording and analysis. The recording electrode was first positioned at a site in the OTid (either multi-unit or single-unit site). Azimuthal and elevational visual tuning curves were run to determine the center of the receptive field. Following this, two azimuthal tuning curves were collected in an interleaved manner (at the best elevation for the site): one curve without AGF microstimulation and the other with AGF microstimulation. Current levels of 5 μA to 25 μA (in steps of 5 μA) were used. At each current level, the data were tested for an effect of AGF microstimulation on the spatial tuning curve. If an effect of AGF microstimulation was detected (Winkowski and Knudsen, 2008), this site was classified as being "valid" and was used for further experimentation (i.e., measurement of competitor strength-response profiles or CRPs). If there was no effect of AGF microstimulation on the spatial tuning curve at any of the current levels, the site was rejected and the recording electrode was moved to a different site.

Multi-unit spike waveforms from a valid recording site were sorted off-line into putative single units ("neurons"), as described previously (Mysore et al., 2011). All recordings in the optic tectum were made in layers 11-13 of the optic tectum (OTid).

Sensory stimuli. Visual and auditory stimuli used here have been described previously (Mysore et al., 2010, 2011). Briefly, visual stimuli were presented on a tangent screen in front of the owl. Looming stimuli were dots that expanded linearly in size over time, starting from a size of 0.6° in radius. The strength (physical salience) of a looming stimulus was controlled by its loom speed. The range of loom speeds tested was within 0 °/s to 16°/s, based on previous experiments showing that the dynamic range of most OTid neurons falls within this range (Mysore et al., 2011).

Auditory stimuli, delivered dichotically through matched earphones, were presented as though from different locations by filtering sounds with head-related transfer functions (Witten et al., 2010). The average binaural levels (referred to as sound levels) of auditory stimuli are indicated in all Figures relative to the minimum threshold, averaged across neurons. The strength of an auditory stimulus was controlled by its level. The range of binaural levels tested was within 0 to 50 dB relative to unit threshold (Mysore et al., 2010, 2011).

The RF and competitor stimuli were presented so that they always occurred within the same hemifield. The relative locations of the RF stimulus, competitor, and the location encoded by the site of electrical microstimulation for all the experiments are plotted in Figs. S1E-F, S2E-F, and S3.

Stimulus presentations without and with AGF microstimulation were always randomly interleaved, with between 10 -15 repetitions in each condition. In Figures 2,3,5, each value of loom speed of the stimulus was repeatedly tested in a randomly interleaved fashion. Similarly, in Figures S1, and S2, each value of ABL of the competitor was repeatedly tested in a randomly interleaved fashion.

Data analysis and statistical methods. All analyses were carried out with custom MATLAB code. The spatial receptive field for each neuron was defined as the set of locations at which a single stimulus evoked responses above baseline. The receptive field locations of the recorded neurons in the OTid and AGF are shown for each set of experiments in Figures S1-S3.

Response firing rates were computed by counting spikes over a time window and converting the resulting count into spikes per second. Across all neurons, the time window used was 200 ms long (median duration; 95 % CI of [200 ms, 225 ms]), and started 100 ms after stimulus onset (median starting time; 95 % CI of [75 ms, 100 ms]). The small differences in the windows reflected a combination of neuron-to-neuron variability in the onset and duration of inhibition by the competing stimulus, and in the effect of the endogenous signal.

Correlations between responses to paired stimuli and the strength of the competitor stimulus were tested using Spearman's rank correlation coefficient (corr command in MATLAB with the Spearman option). Neurons that did not show a significant correlation ($p>0.05$, correlation test) in the "no microstimulation" condition were omitted from further analysis. For the remaining neurons (analyzed in Figures 1-3, 7, and Supp. Fig. 3), CRPs were fit with a standard sigmoidal function using a nonlinear least squares estimation procedure (*nlinfit* command in MATLAB). CRP data were collected only at "valid" recording sites (see "Site selection" above). At valid sites, almost all CRPs exhibited a significant correlation with competitor strength and, therefore, only a small number of neurons were omitted from analysis. The numbers of omitted neurons for the analyses in the different figures are as follows: 1/16 (Fig. 1A-D), 1/11 (Fig. S1A-D), 3/26 (Fig. 2A-D), 2/23 (Fig. S2A-D), 0/14 (Fig. 3A-D).

The transition range of a CRP was defined as the range of competitor strengths over which responses dropped from 90% to 10% of the total range of responses (Mysore et al., 2011). The range of responses was estimated by using the sigmoidal fits to the data to determine the minimum and maximum response levels over a standard range of competitor strengths loom-speeds (0 °/s to 18°/s for looming competitors, and 0 to 50 dB re. threshold for auditory competitors; Mysore et al., 2011). Switch-like response profiles were defined as those for which the transition range was sufficiently narrow (≤ 4°/s for looming competitors; ≤ 10 dB for auditory competitors; Mysore et al., 2011).

<u>*Ensemble code.*</u> To construct an estimate of the OTid ensemble code, we adopted an approach utilized in previous reports (Mysore and Knudsen, 2011; Niessing and Friedrich, 2010). Briefly, the responses to the competition protocol of 15 RF-neurons and 14 competitor-neurons were combined into a matrix (columns = neurons, rows = strengths of the competitor stimulus). Each column of this matrix represented an estimate of the pattern of activity across the OTid population to a particular strength of the competitor stimulus. To ensure fair combination of data across neurons, the fixed strength of the RF stimulus for each neuron was first aligned (x-shifted) to the population average of 7.2 °/s; we have shown previously that x-shifts in the data that occur due to this normalization do not affect the transition range of the responses (Mysore et al., 2011). We then re-sampled the responses of each neuron at competitor stimulus strengths between 0 and 16 °/s (in steps of 2°/s) using a polynomial, shape-preserving, piecewise cubic interpolation (interp1 command in MATLAB with the 'pchip' method; this method interpolates using local values of the data). The firing rates of each neuron were mean-

subtracted and then normalized to the population maximum, such that positive values represent responses greater than the mean, while negative values represent responses less than the mean.

Pair-wise correlations between the rows (activity patterns) of the ensemble activity matrix were quantified using the Pearson correlation coefficient. A horizontal transect through this correlation matrix showed how the correlations changed as a function of competitor strength.

Categorization index. Two stimulus categories were represented in the ensemble code, as evident in the abrupt changes in the correlation matrix (and the horizontal transects). The category boundary (Fig. S3D,G: dashed vertical line), signaling whether the RF stimulus was the highest priority stimulus or not, corresponded to the strength of the competitor at which the abrupt change in correlation values was observed. In the absence of the endogenous influence, the category boundary was between 6°/s and 8°/s (nearly equal to the strength of the RF stimulus of 7.2 °/s; Fig. 3C; Fig. S3D).

The quality of categorization by the ensemble code was quantified using a *categorization index* (Freedman and Assad, 2006; Mysore and Knudsen, 2011) that compared two metrics: (i) the average within-category difference in response correlations (WCD), and (ii) the average between-category difference in response correlations (BCD). The categorization index was defined as (BCD-WCD)/(BCD+WCD), with positive values of the index indicating larger differences between categories than within a category, and thereby revealing a categorical representation, and negative values of the index indicating smaller differences between categories than within a category. Higher values of the index signify better quality categorization.

WCD and BCD values were calculated as follows (Freedman and Assad, 2006; Mysore and Knudsen, 2011). For calculating WCD, differences in response correlations were computed between stimulus pairs *within* a category for which the strengths of the competitors were separated by 2°/s, 4°/s, 6°/s, etc (for instance, Fig. S3 D2-D4, E2-E4; dotted black lines). In contrast, for calculating BCD, differences in response correlations were computed between stimulus pairs that *straddled* the category boundary for which the strengths of the competitors were separated by 2°/s, 4°/s, 6°/s, etc (for instance, Fig. S3 D2-D4, E2-E4; solid black lines). Note that any given strength separation could be achieved by multiple combinations of stimulus pairs (Fig.S3E,H). For instance, for the response profile in the bottom panel of Figure S3E, with the category boundary lying between competitor strengths of 6 °/s and 8 °/s, a strength separation of 4 °/s can be computed between responses to five within-category stimulus pairs (Fig. S3 D1-D2): with competitor strengths of (0°/s, 4°/s), (2°/s, 6°/s), (8°/s, 12°/s), (10°/s, 14°/s), and (12°/s, 16°/s).

In order for the comparison of WCD and BCD to be valid, it is necessary that the following two constraints be satisfied during the calculation of WCD and BCD: (i) only those strength separations are included that are represented in both WCD and BCD calculations, and (ii) both calculations include equal numbers of stimulus pairs for each value of strength separation. To satisfy the first constraint, strength separations larger than 8°/s were not included in the calculation because no such separations can be found for the WCD calculation (Fig. S3 D3, G3; including such separations in the BCD calculation would unfairly bias the BCD towards larger values). To satisfy the second constraint, WCD and BCD values for the response profile in Figure 3F (bottom panel) were calculated using a total of 7 pairs corresponding to 4 strength separations (Fig. S3E): 2 °/s (1 pair), 4 °/s (2 pairs), 6 °/s (3 pairs), and 8 °/s (1 pair). Similarly, WCD and BCD values corresponding to Fig. 3H were calculated using 7 pairs (Fig. S3H). Because many more pairs than the allowed number can exist for a given strength separation (for instance, the number of possible within-category pairs for a strength separation of 4°/s is five whereas the allowed number is two; Fig. S3E, column 1 vs. column 3), the WCD calculation was performed by choosing for each strength separation the allowed number of pairs at random from the total number of possible pairs, and repeating the calculation many times (Monte Carlo simulation, N=1000 repetitions). The same procedure was adopted for the BCD calculation. Reported are the mean values of WCD and BCD; their mean ± s.e.m values are plotted in Fig. S3I.

Discriminability. Discriminability was computed using the metric d', defined for the distributions of responses to two stimulus conditions, as $(m_1-m_2)/\sqrt{(s_1*s_2)}$, where m_1 and m_2 are the means, and s_1 and s_2, the standard deviations, of the two sampled distributions.

Statistical testing. Parametric or non-parametric, paired statistical tests were applied based on whether the distributions being compared were Gaussian or not (Lilliefors test of normality); tests were two-tailed. The Holm-Bonferroni correction for multiple comparisons was applied when appropriate. Data shown as a ± b refer to mean ± s.e.m. The '*' symbol indicates significance at the 0.05 level. In statistically comparing the data across the two experimental conditions (no stimulation and AGF stimulation), the experimenter was not blind to the experimental conditions to which the data sets belonged.

To test whether AGF microstimulation had a significant effect on the parameters of the CRP, the Wald F-test was used as follows. For the CRP obtained with microstimulation, two different sigmoidal fits were obtained. In case I ("best unconstrained fit"), all four parameters of the sigmoidal equation were free parameters and the best fit was obtained. In case II ("best constrained fit"), the parameter "s_{50}" of the sigmoidal equation was fixed to the s_{50} value of the CRP obtained without microstimulation, while the other three parameters were free parameters. In both cases, the residual sums of squares were computed as rss_1 and rss_2, respectively. The number of free parameters in the two cases were p_1=4 and p_2=3, respectively. The number of data points in each CRP was n=9. An F-statistic was calculated (as below). The effect of AGF microstimulation on s_{50} was deemed significant if the F-statistic was greater than the critical value of an F-distribution with (p_1-p_2, n-p_1) degrees of freedom calculated for α=0.05. The same procedure was applied to test for significant effects on the other three parameters of the sigmoid as well.

$$F = \frac{\left(\frac{RSS_2 - RSS_1}{p_1 - p_2}\right)}{\left(\frac{RSS_1}{n - p_1}\right)} \quad (4)$$

Computational modeling. The standard sigmoidal equation, the hyperbolic ratio function, was used to describe OTid and Imc responses to varying loom speeds of a single RF stimulus based on experimental measurements in these two areas (Mysore and Knudsen, 2012) (eqn. 1 in the text). For OTid units, the values of the four parameters were chosen such that the resulting equation yielded the best sigmoidal fit to the experimentally measured, average loom speed-response function (Mysore and Knudsen, 2012): c=5.3, h=22.2, s_{50}=11.6, m=2. For Imc units, the parameters were chosen to be c=5, h=15, s_{50}=8, m=3 based on published work(Mysore and Knudsen, 2012) showing that these values lie within the range of values for which the output of the model with the two-stimulus competition protocol (exogenous stimuli only) matches the responses of OTid neurons measured experimentally.

The divisive inhibitory effect of the Imc on the responses of OTid neurons was modeled as a combination of both input and output division of the single stimulus-response function (eqn. 2 in the text; described in detail in previous work (Mysore and Knudsen, 2012)). In this equation, s_{in} and s_{out} are input and output divisive influences, respectively, which increase as the strength of the competitor increases (Mysore et al., 2011; Mysore and Knudsen, 2012), and were taken to be proportional to the steady-state activity r_{imc}^{ss} of the inhibitory units driven by the competitor:

$$s_{in} = d_{in} \bullet r_{imc}^{ss}, \quad s_{out} = d_{out} \bullet r_{imc}^{ss} \quad (5)$$

Here, d_{in} and d_{out} are input and output divisive parameters (Mysore and Knudsen, 2012). The value of r_{imc}^{ss} was obtained as the value at which the reverberatory activity of Imc units settled (change < 5% in subsequent iterations). This reverberatory activity was a result of the reciprocal inhibitory connectivity within the Imc, modeled, as in previous work (Mysore and Knudsen, 2012), also as a combination of input and output division:

$$r_{imc}(t) = \left(\frac{1}{i_{out}(t)+1}\right) \cdot \left(\frac{c}{i_{in}(t)+1} + h\left(\frac{l^n}{l^n + s_{50}^n + (i_{in}(t))^n}\right)\right) \quad (6)$$

The input and output divisive influences at time-step t, $i_{in}(t)$ and $i_{out}(t)$, respectively, were modeled, as in previous work (Mysore and Knudsen, 2012), as being proportional to the activity of the inhibitory units at the previous time-step (similar to eqn. 3):

$$i_{in}(t) = q_{in} \cdot r_{imc}(t-1), \quad i_{out}(t) = q_{out} \cdot r_{imc}(t-1) \qquad (7)$$

The values of various parameters were chosen based on published work (Mysore and Knudsen, 2012) to be: d_{in} = 0, d_{out}=0.06 (eqn 3), and q_{in}=0.84, q_{out}=0.01 (eqn. 7), because they are within the range of values for which the output of the model matched well the responses of OTid neurons measured experimentally, using the two-stimulus competition protocol (without AGF stimulation).

Gain control of OTid (and Imc) responses by aligned AGF microstimulation were modeled as a combination of input and response multiplication of the single-stimulus, loom speed-response functions (eqn. 3 in the text), following published work (Williford and Maunsell, 2006; Winkowski and Knudsen, 2008). In this equation, m_{in} and m_{out} are free parameters of the model, representing input and response multiplicative gain, respectively, with m_{in} taking values ≤ 1 (m_{in}=1 represents no input multiplicative influence, lower m_{in} values represent more powerful input multiplication), and m_{out} taking values ≥ 1 (m_{out}=1 represents no response multiplicative influence; higher m_{out} values represent more powerful response multiplication).

For the simulations in Figures 5 and 6, the range of m_{in} values explored was [0.25,1]. This range was chosen because it was more than wide enough to account for the experimentally reported leftward shifts of single stimulus-response functions in the OTid following aligned AGF microstimulation (Winkowski and Knudsen, 2008). The largest leftward shift of the OTid single stimulus-response function produced within this range of m_{in} values was 5.8 °/s (produced by m_{in} = 0.25). This corresponds to 26% of the dynamic range of loom speeds for OTid neurons (or 50% of the original s_{50}; (Mysore et al., 2011)). By comparison, the average leftward shift due to aligned AGF microstimulation that has been reported experimentally is about 9% of the dynamic range (Winkowski and Knudsen, 2008).

The range of m_{out} values explored was [1,2.1], chosen also because it was more than wide enough to account for the experimentally observed increases in the maximum firing rates of single stimulus-response functions following aligned AGF microstimulation. The largest increase in the maximum firing rate of the OTid single stimulus-response function produced within this range of m_{out} values was an increase of 24 sp/s (produced by m_{out} = 2.1). This corresponds to a 110% increase in the maximum firing rate. By comparison, the average change in the maximum firing rate of strength-response functions due to aligned AGF microstimulation that has been reported experimentally is only about 5% (Winkowski and Knudsen, 2008). Because the same ranges of m_{in} and m_{out} values were used to test the effects of both AGF→ OTid and AGF→ Imc gain modulation in simulations, the chosen ranges allowed for a broad exploration of the AGF→Imc multiplicative gain factors.